Desalination and Water Treatment
www.deswater.com
doi: 10.1080/19443994.2014.940394

56 (2015) 475–484
October

Taylor & Francis
Taylor & Francis Group

Adsorption of tannic acid from aqueous solution by aminopropyl functionalized SBA-15

Jingliang Liu[a,*], Huan Chen[b], Zhaoyi Xu[c], Shourong Zheng[c], Mengwei Xue[a]

[a]*School of Biochemical Environmental and Engineering, Nanjing XiaoZhuang University, Nanjing 211171, P.R. China, Tel. +86 025 8617 8308; email: liujingliangnju@163.com (J. Liu), Tel. +86 138 1409 0304; email: xmw1102@sina.com (M. Xue)*
[b]*School of Environmental and Biological Engineering, Nanjing University of Science and Technology, Nanjing 210094, P.R. China, Tel. +86 137 7070 3704; email: hchen404@mail.njust.edu.cn*
[c]*State Key Laboratory of Pollution Control and Resource Reuse, and School of the Environment, Nanjing University, Nanjing 210093, P.R. China, Tel. +86 025 8968 0370; emails: zhaoyixu@nju.edu.cn (Z. Xu), srzheng@nju.edu.cn (S. Zheng)*

Received 23 January 2014; Accepted 16 June 2014

ABSTRACT

Tannic acid (TA) is generally considered as one of the refractory organic pollutants in water. In this study, aminopropyl functionalized SBA-15 (SBA-15-NH_2) was prepared by post-grafting method and the adsorption behavior of TA on the synthetic adsorbent was investigated using batch experiments and adsorption kinetic tests. The adsorbent was characterized by a variety of experimental and spectroscopic techniques with respect to structural, porosity, and surface characteristics. Characterization results showed that SBA-15-NH_2 has ordered mesoporous structure, BET surface area of 245.49 m^2/g, and the pore volume of 0.43 cm^3/g. Batch adsorption tests showed that SBA-15-NH_2 adsorbent exhibited high adsorption affinity to TA with a maximum adsorption capacity of 272.4 mg/g. TA adsorption over the adsorbents could be well described by Freundlich adsorption model, suggesting that the adsorption process is heterogeneous. The hydrogen bonding ability and electrostatic interaction between the TA and aminopropyl groups further conformed by pH and ionic strength experiments. In addition, the adsorption process obeyed the pseudo-second-order kinetics and the rate constant decreased with initial TA concentration.

Keywords: Tannic acid; Adsorption; SBA-15; Aminopropyl functionalized

1. Introduction

Tannic acid (TA) is one of the naturally occurring polyphenolic compounds, which is generated by decomposing the organic matter [1]. Also, TA can be released from the timber processing, paper, and leather factory [1,2]. The existence of TA in surface water and ground water may cause taste and odor problems. Furthermore, TA would influence the species and microorganism in water due to its toxicity [3]. For example, TA may interact with chlorinated disinfectants and form disinfection byproducts, which are highly carcinogenic [4,5]. Therefore, it is highly desirable to develop effective treatment methods for TA removal from aqueous solution.

Many treatment methods [2,6–9], such as filtration, adsorption, biological treatment, electrochemical method et al. have been used to remove the TA from water. Among these methods, adsorption treatment

*Corresponding author.

has been considered as a simple and effective method to remove TA from the aquatic environment. Various adsorbents have been reported to remove the TA from water in previous studies [8–13]. For example, Rivera-Utrilla et al. [10] studied the adsorption of TA to three activated carbons and the adsorption amount varied from 54.2 to 96.2 mg/g. Anirudhan et al. [11] studied the adsorption of TA to cationic surfactant-modified bentonite clay and observed high removal efficiency, which caused by the high surface area and porosity associated with organoclay.

Recently, mesoporous silica has been considered as an alternative candidate for adsorptive removal of pollutants from water because of the high surface area, ordered mesoporous structure, and narrow pore size distribution. The ordered mesoporous silica which first synthesized in 1992 [14,15] has attracted broad attention due to the large surface area and high pore volume. Mesoporous SiO_2 may expand the application in separation, catalysis, and adsorption processes for ordered inert matrix and surface functionalization [16]. It is worth mentioning that mesopours SiO_2 contains abundant surface silanol groups, which are susceptible to surface functionalization [17–21]. It is hypothesized that amino functionalized mesoporous SiO_2 prepared by the grafting method may have high exposure of surface functionality, and display superior performance for TA adsorption. For example, Tao et al. [22] studied the humic acid adsorption to aminopropyl functionalized mesoporous silica and reported high removal efficiency. However, to our best knowledge, thus far few studies [23–25] have been conducted on adsorption of aqueous TA to surface functionalized mesoporous silica.

The objective of this study is to explore the aminopropyl functionalized SBA-15 for adsorptive removal of TA in water. Aminopropyl functionalized SBA-15 adsorbent was prepared by the post-grafting method and characterized by X-ray diffraction (XRD), infrared spectroscopy, transmission electron microscopy, X-ray photoelectron spectroscopy (XPS), N_2 adsorption/desorption isotherms, and zeta potential measurements. TA adsorption to the adsorbents was investigated using the batch experiments and adsorption kinetic tests. The impacts of pH and ionic strength on TA adsorption were also investigated.

2. Materials and methods

2.1. Materials

TA (Sigma-Aldrich) and 3-aminopropyltrimethoxysilane (Sigma) were supplied by Aldrich Chemical Co. Other chemicals purchased from Nanjing Chemical Reagents Co., Ltd, which were used as received and at least analytical grade.

2.2. Preparation of materials

SBA-15 was prepared using Pluronic P123 as the structure-directing agent and tetraethoxysilane (TEOS) as the silica source [20]. Briefly, 8.0 g of Pluronic P123 (Aldrich) was dissolved in 300 mL of 2.0 M HCl solution at 40˚C and then 17.6 g of TEOS (98%, Shanghai Chemical Co.) was added. After stirring at 40˚C for 24 h, the solution was transferred to a Teflon-lined autoclave which was kept at 100˚C for 24 h. The resulting material was recovered by filtration and washed with deionized water several times. The organic template (Pluronic P123) was removed by calcination at 550˚C for 6 h under air.

Aminopropyl functionalized SBA-15 was prepared by the post-grafting method using 3-aminopropyl-trimethoxysilane as the silylation agent. Briefly, 3.0 g of SBA-15 and 50 mL of toluene were added to a 250 mL three-necked flask and ultrasonically dispersed for 10 min. Three milliliter of 3-aminopropyl-trimethoxysilane was then added into the flask, and then the mixture was refluxed at 85˚C with continuous stirring for 8 h. The resulting functionalized SBA-15 was gathered by filtration and soxhlet extraction with isopropyl alcohol for 8 h followed by washing with ethanol, and drying at 60˚C under vacuum for 12 h. The materials obtained are referred to as SBA-15-NH_2.

2.3. Characterization of materials

XRD patterns of the samples were collected in a range of small angle 0.5–5˚C from a Rigaku D/max-RA powder diffraction-meter (Rigaku, Japan) using Cu Kα radiation. TEM images of the samples were recorded with a JEM-200CX electron microscope. The zeta potentials were measured by a Zeta Potential Analyzer (Zeta PALS, Brookhaven Instruments Co.). Briefly, 30 mg of the catalysts were dispersed in 1 L KCl solution (10^{-3} M). The solution pH was then adjusted by 0.1 M HCl or 0.1 M NaOH and the suspension was equilibrated for 24 h prior to measurement. N_2 adsorption/desorption isotherms of samples were obtained on a Micrometrics ASAP 2020 (Micromeritics Instrument Co., USA) apparatus at −196˚C (77 K). The XPS was conducted on a PHI5000 VersaProbe equipped with a monochromatized Al *Ka* excitation source ($h\upsilon = 1486.6$ eV) (ULVAC-PHI, Japan). The C1s peak (284.6 eV) was used for the calibration of binding energy. Elemental analysis was performed using an elemental analyzer of Vario MICRO (Elementar,

Germany) to determine the C, H, and N contents. Thermogravimetric analysis was measured using a thermal analyzer of Pyris 1 DSC (PerKinElmer Co., USA) to quantify the amount of organic components.

2.4. Adsorption

TA adsorption isotherms were performed by batch adsorption experiments. Briefly, 10 mg of adsorbent was introduced into 40 mL glass vials equipped with polytetrafluoroethylene-lined receiving 40 mL of TA solution with varied intial concentrations. The pH of aqueous solution was adjusted with 0.01 M HCl and 0.01 M NaOH. The samples were covered with aluminum foil and mixed end-over-end at room temperature for 24 h. After centrifugation, the residual solute was determined using UV–vis spectrometer with detecting wavelength at 278 nm [1]. Calibration curves were obtained separately from control samples receiving the same treatment as the adsorption samples, but without the absorbent. The equilibrium adsorption amounts of TA were calculated according to the following equation:

$$q_e = \frac{(C_0 - C_e)V}{M} \quad (1)$$

where q_e is the equilibrium adsorption amount, C_0 is the initial TA concentration, C_e is the equilibrium concentration, V is the solution volume and M is the adsorbent mass.

Separate sets of experiments were conducted to test the effects of pH and ionic strength. In the pH experiments, 10 mg of SBA-15-NH_2 and 40 mL of 25 mg/L TA solution with different pH was preadjusted using 0.01 M HCl and NaOH to ensure the desired pH at adsorption equilibrium. In the ionic strength experiments, adsorption was performed using background solutions of 0.01, 0.02, 0.05, and 0.1 M NaCl, KCl, or $CaCl_2$. After adsorption equilibrium, the residual TA concentrations were determined and adsorption amounts of TA were calculated according to Eq. (1).

Additional single batch experiments were conducted to assess the adsorption kinetics. Typically, 0.1 g of SBA-15-NH_2 was added into a 500 mL flask containing 500 mL of 30, 60, or 120 mg/L of TA solution using magnetic stirred vigorously in a thermostatic incubator at 25℃. About 3 mL of sample was taken out from the flask at predetermined time intervals. The adsorbent was separated from solution by filtration using 0.45 μm filters, and the residual concentration of TA in the solution was determined spectrophotometrically. Calibration curves were obtained separately from controls receiving repeated sampling in the same time intervals. The equilibrium pH of all samples (except for the pH experiments) was 7.5 ± 0.2.

3. Results and discussion

3.1. Characterization of adsorbent

The small-angle XRD patterns of SBA-15 and SBA-15-NH_2 are displayed in Fig. 1. The peaks with 2θ at 0.89˚, 1.55˚, and 1.77˚ were indexed to the (110), (100), and (200) diffraction, reflecting the ordered mesoporous structure of SBA-15 with p6 mm hexagonal symmetry [26,27]. As for SBA-15-NH_2, the intensive (100) and weak (110) and (200) peaks were also observed, reflecting the presence of ordered hexagonal structure similar to the SBA-15. However, aminopropyl functionalization led to the decrease of peak intensity, likely due to the contrast matching between the SiO_2 framework and aminopropyl groups grafted to SBA-15 surface [28,29]. The ordered pore structures of SBA-15 and SBA-15-NH_2 with uniform dimension and hexagonal arrangement could also be clearly visualized by TEM images (See Fig. 2).

N_2 adsorption/desorption isotherms and the pore size distributions of the samples are presented in Fig. 3. For all the adsorbents, typical capillary condensation was observed within a relative pressure range of 0.6–0.9, reflecting the presence of mesoporous. BET surface areas and pore volumes of the samples are listed in Table 1. The BET surface areas of the samples were 626.37 and 245.43 m^2/g for SBA-15 and SBA-15-NH_2, respectively, reflecting decreased surface area with functionalization in SBA-15-NH_2. Compared with

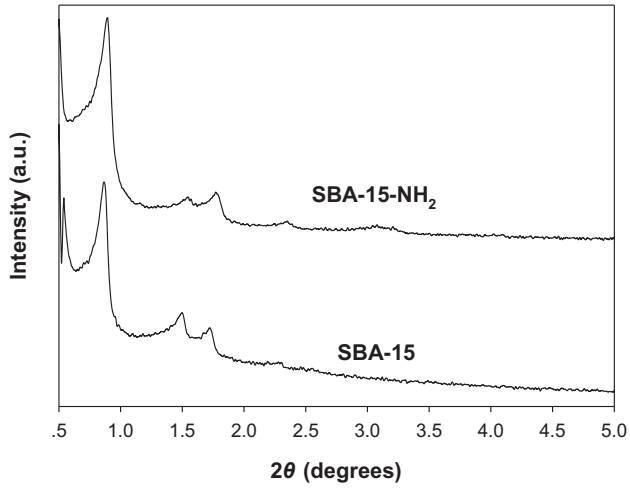

Fig. 1. XRD patterns of SBA-15 and SBA-15-NH_2.

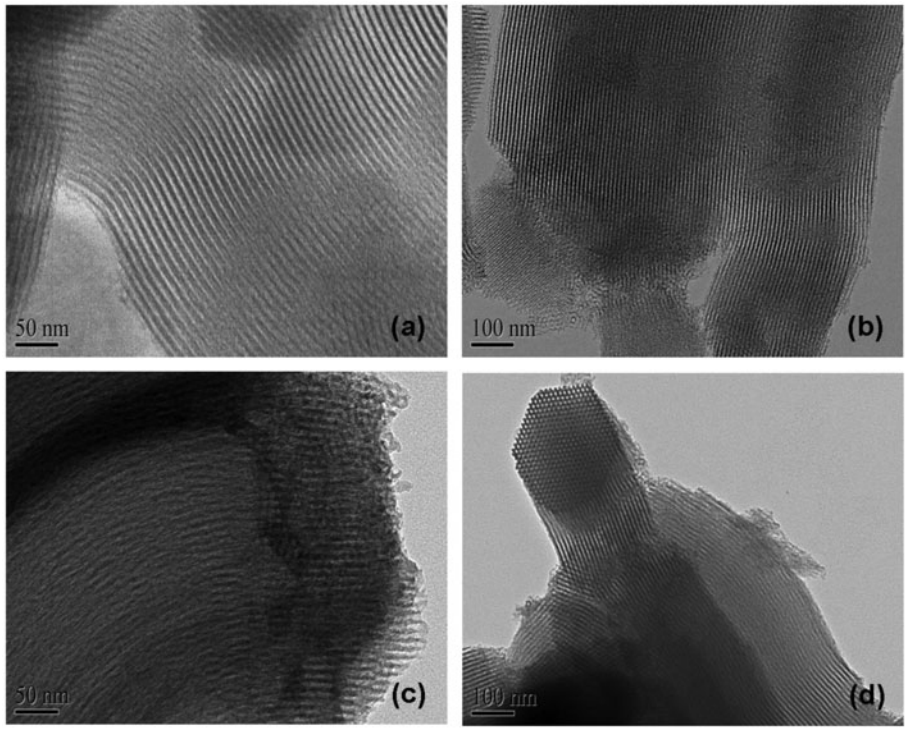

Fig. 2. TEM images of the SBA-15 (a) (b) and SBA-15-NH_2 (c) (d).

SBA-15, SBA-15-NH_2 presented decreased pore volume (0.43 cm^3/g). As shown in Fig. 3(b), the maximum pore size distributions of SBA-15-NH_2 was shifted to small pore, indicating the deposition of -NH_2 in the pore channel. Moreover, the deposition of 3-aminopropyltrimethoxysilane reduced the differential pore volume at the maximum pore size distribution, reflecting the decreased ordering of mesostructured phase in SBA-15-NH_2 [22].

The IR spectra of SBA-15, SBA-15-NH_2 and after adsorption of TA SBA-15-NH_2-TA are presented in Fig. 4. For SBA-15, the bands at 1,081, 962, 804, and 460 cm^{-1} were characteristic of the stretching and deformation vibrations of SiO_2. The band at 1,635 cm^{-1} was assigned to the bending vibration of surface hydroxide and the broad peak around 3,440 cm^{-1} was assigned to hydrated silanol groups. For SBA-15-NH_2, the grafted amino groups to the SBA-15 were identified by the stretching vibration of methylene groups at the peak around 2,940 cm^{-1} and the bending vibration of amino groups at the peak around 1,550 cm^{-1}. After adsorption of TA the intensity of the two peaks was decreased (see the two peaks of SBA-15-NH_2-TA in Fig. 4) reflecting the interaction between amino group and TA.

Zeta potentials of SBA-15 and SBA-15-NH_2 are displayed in Fig. 5. Clearly, the zeta potentials decreased at a pH range from 3.0 to 7.0, and changed slightly at higher pH for both of the samples. The isoelectric point (IEP) of SBA-15 was found to be 1.9, which was identical to that of amorphous SiO_2 [30]. The IEP for SBA-15-NH_2 was around 5.8, which indicated that aminopropyl groups led to increased IEP [31]. As the p*K*a value of primary amine group is around 9.8 [32], it was suggested that aminopropyl group successfully grafted onto SBA-15 and aminopropyl functionalization led to the increased IEP. Consistent results were also observed from the IR spectra.

XPS analysis is a surface sensitive technique which can analyze the chemical valence of surface elements and provide the compositions of surface elements. The XPS N1s spectra of SBA-15-NH_2 is presented in Fig. 6. As shown in Fig. 6, the diffraction peaks with binding energy at 398.9 and 400.8 eV were assigned to neutral amino (-NH_2) and protonated amino groups (NH_3^+), respectively. The presence of NH_3^+ may be caused by the hydrogen bonding interaction between surface -NH_2 and surface silanol groups [33]. Thermogravimetric analysis is displayed in Fig. 7. The surface atomic content and elemental composition of SBA-15-NH_2 are listed in Table 1. The results of elemental analysis showed the content of SBA-15-NH_2 C, H, N were 9.18, 2.82, and 3.42 wt.%. The total amount is 15.42%, which is consistent with thermogravimetric

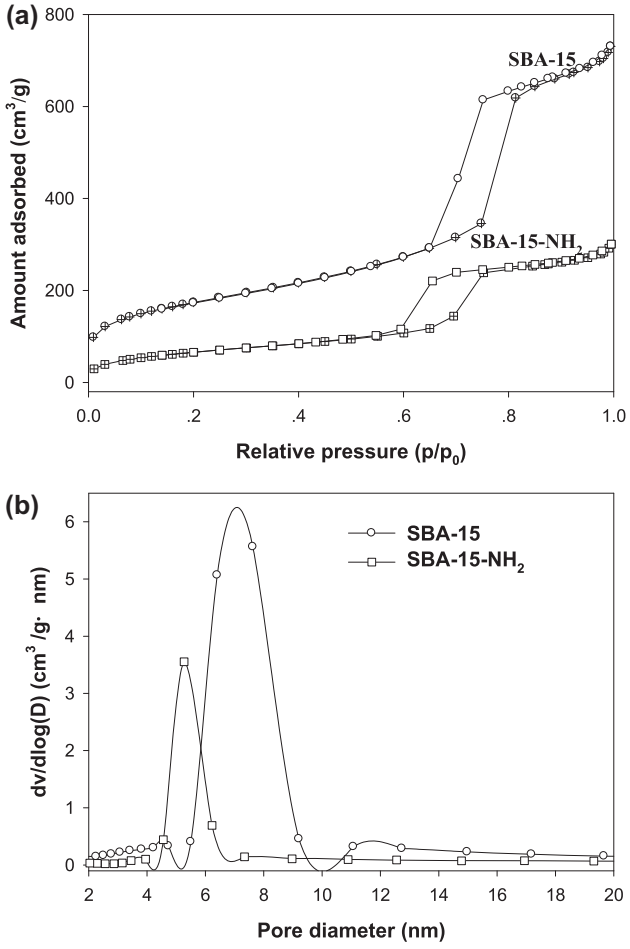

Fig. 3. (a) N_2 adsorption/desorption isotherms and (b) pore size distributions of the samples.

analysis results 15.74% (See the weight loss from 100 to 700℃ in Fig. 7). It could be seen from Table 1 that the content of N determined by XPS did not disagree with the results tested by elemental analyzer. It is demonstrated that the distribution of aminopropyl groups by post-grafting method was heterogeneous.

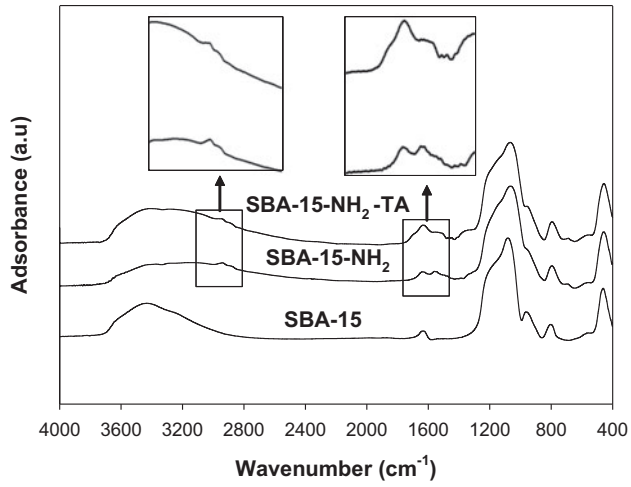

Fig. 4. IR spectra of SBA-15, SBA-15-NH_2 and SBA-15-NH_2-TA.

3.2. Adsorption isotherms

TA adsorption isotherms on SBA-15 and SBA-15-NH_2 at 25℃ and pH 7.5 are compared in Fig. 8. Clearly, SBA-15 exhibited negligible adsorption for TA. While the TA adsorption amounts over SBA-15-NH_2 sharply increased and the maximum adsorption amount within the tested concentration range was 218.2 mg/g. The substantially enhanced adsorption of TA on SBA-15-NH_2 was probably due to the hydrogen bonding ability and electrostatic interaction between the TA and the aminopropyl groups. The relative importance of these two adsorption mechanisms was further discussed based on the results of pH adsorption (see below).

The adsorption data were fitted to the Freundlich model ($q_e = K_F C_e^{1/n}$), where q_e (mg/g) and C_e (mg/L) are the adsorbed concentration and aqueous concentration at adsorption equilibrium, respectively. K_F (mg^{1-n} L^n/g) is the Freundlich affinity coefficient; n is

Table 1
Specific surface area, pore volume parameters, surface atomic content and elemental composition for adsorbents

Adsorbent	S_{BET}[a] (m^2/g)	V_t[b] (cm^3/g)	Surface atomic content[c]		Elemental composition		
			C1s (%)	N1s (%)	C (%)	H (%)	N (%)
SBA-15	626.37	1.08	/	/	/	/	/
SBA-15-NH_2	245.49	0.43	85.74	14.26	9.18	2.82	3.42

[a]Determined by N_2 adsorption using the Brunauer–Emmett–Teller (BET) method.
[b]Total pore volume, determined at $P/P_0 = 0.976$.
[c]Determined by XPS.

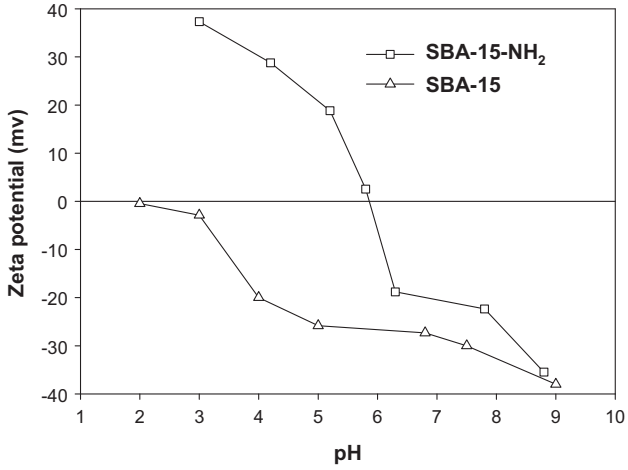

Fig. 5. Zeta potentials of SBA-15 and SBA-15-NH_2 as a function of solution pH.

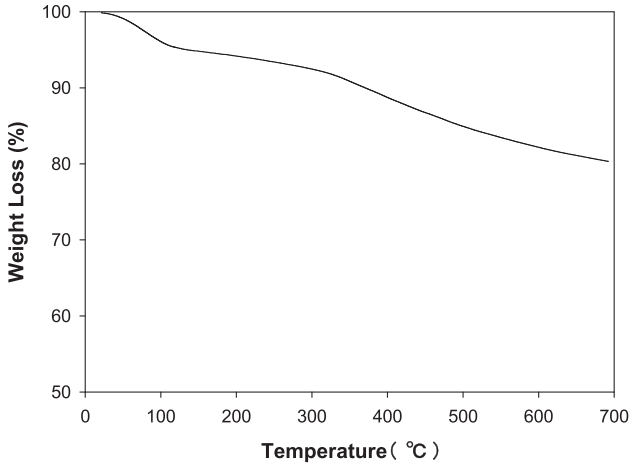

Fig. 7. Thermogravimetric analysis curves of of SBA-15-NH_2.

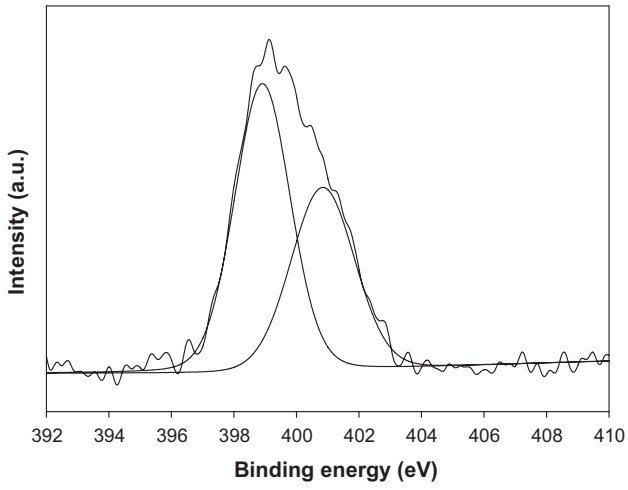

Fig. 6. XPS N1s spectra of SBA-15-NH_2.

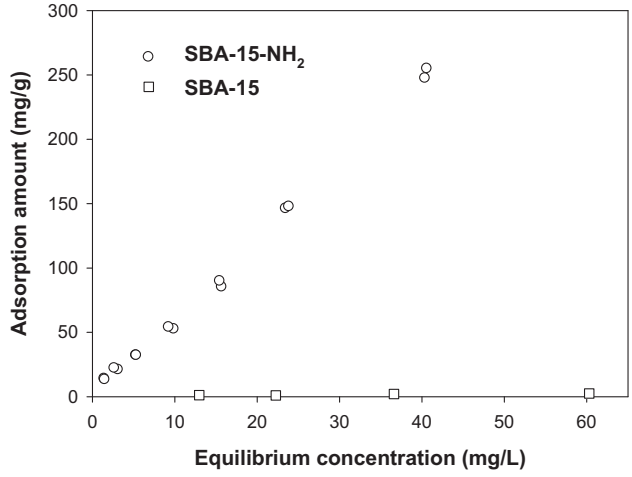

Fig. 8. Adsorption isotherms of TA over SBA-15 and SBA-15-NH_2 plotted as equilibrium adsorption amount vs. equilibrium concentration.

the Freundlich linearity index. The fitting parameters for TA adsorption isotherms using Freundlich equation are summarized in Table 2. TA adsorption on SBA-15-NH_2 could be well described by the Freundlich adsorption model with R^2 higher than 0.96. Moreover, it is further confirmed that heterogeneous distribution of aminopropyl groups anchored on the SBA-15, which is in accordance with previous studies [34,35]. In order to verify the heterogeneity of the amino groups, pore size distribution of SBA-15-NH_2 with and without TA adsorption is compared in Fig. 9. Clearly, the pore volume was decreased after adsorption of TA, but the pore was slightly occupied after adsorption of TA reflecting very little aminopropyl groups grafting in the pore. It is consistent with the characterization results, the content of N designed by XPS inconformity with the element analysis (see Table 1).

Table 2
Freundlich model parameters, K_F, n and R^2 for adsorption of TA to the adsorbents

Adsorbent	K_F (mg $^{1-n}$ L^n/g)	n	R^2
SBA-15	0.44	0.37	0.56
SBA-15-NH_2	8.08	0.89	0.97

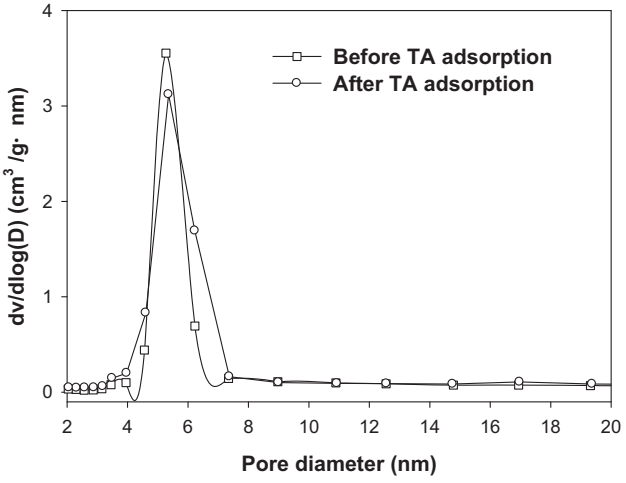

Fig. 9. Pore size distributions of SBA-15-NH_2 before and after TA adsorption.

3.3. Adsorption kinetics

TA adsorption to SBA-15-NH_2 with initial concentrations of 30, 60, and 120 mg/L are complied in Fig. 10. TA adsorption amounts on SBA-15-NH_2 increased rapidly at the initial 30 min and slowly at subsequent 100 min according to the Fig. 10. In addition, adsorption equilibrium was almost achieving within 200 min. To evaluate the mass transfer process during the TA adsorption, the pseudo-first-order and pseudo-second-order kinetic models were applied. Lagergren's rate equation was usually used to describe the pseudo-first-order kinetics [36]:

$$\log(q_e - q_t) = \log(q_e) - k_1 t/2.303 \quad (2)$$

The pseudo-second-order kinetics model can be expressed as follows [37]:

$$t/q_t = 1/(k_2 q_e^2) + t/q_e \quad (3)$$

where q_e is the equilibrium adsorbed concentration, q_t is the adsorbed concentration at time t, k_1 and k_2 are the pseudo-first order rate constant and the pseudo-second order rate constant, respectively.

Simulation results of TA adsorption to SBA-15-NH_2 based on the pseudo-first-order kinetics and pseudo-second-order kinetics are displayed in Fig. 11 and the fitting parameters are listed in Table 3. As shown in Fig. 11 (b), the plot of t/q_t vs. t presented linear relation with higher R^2 (0.999), suggesting that pseudo-second-order kinetic model could well depict TA adsorption process to SBA-15-NH_2. In addition, TA adsorption amounts (q_{exp} see Table 3) obtained from experimental data were approximately identical to the data that calculated from pseudo-second-order model (q_{cal} see Table 3), further confirming that TA adsorption process on SBA-15-NH_2 obeyed pseudo-second-order kinetics model.

The rate constants (k_2) of TA adsorption on SBA-15-NH_2 were found to be 4.83×10^{-3}, 9.94×10^{-4}, and 8.60×10^{-4} g/(mg·min) at initial TA concentration of 30, 60, and 120 mg/L, respectively (see Table 3), indicative of a relatively slower adsorption process at higher TA adsorption amount. This is probably

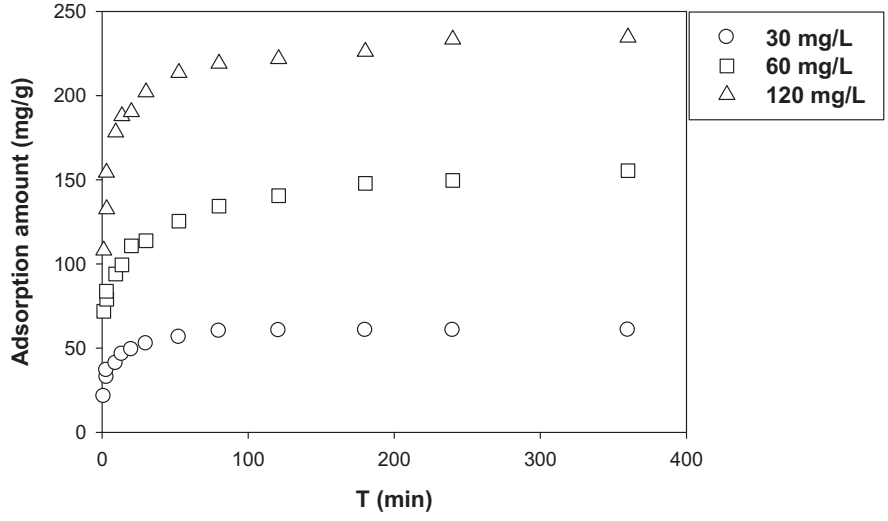

Fig. 10. Time resolved TA adsorption to SBA-15-NH_2 at different initial TA concentrations.

Table 3
Fitting parameters for adsorption kinetics by pseudo-first-order and pseudo-second-order models

		First order kinetics			Second order kinetics		
C_0 (mg/L)	q_{exp} (mg/g)	k_1 (1/min)	q_{cal} (mg/g)	R^2	k_2 (g/(mg·min))	q_{cal} (mg/g)	R^2
30	60.75	4.9×10^{-3}	19.50	0.89	4.83×10^{-3}	61.34	0.99
60	155.41	2.13×10^{-3}	65.21	0.96	9.94×10^{-4}	156.25	0.99
90	234.56	2.99×10^{-3}	73.28	0.91	8.60×10^{-4}	238.10	0.99

because at a low TA concentration, the TA molecules reaching the surface of the adsorbent would be quickly anchored to the adsorption active sites located in the pore mouth region and adjoining region. However, at a higher initial concentration, TA molecule was adsorbed deeply into the pore to approach aminopropyl groups by penetrating through a relatively long diffusion path, leading to a low adsorption rate.

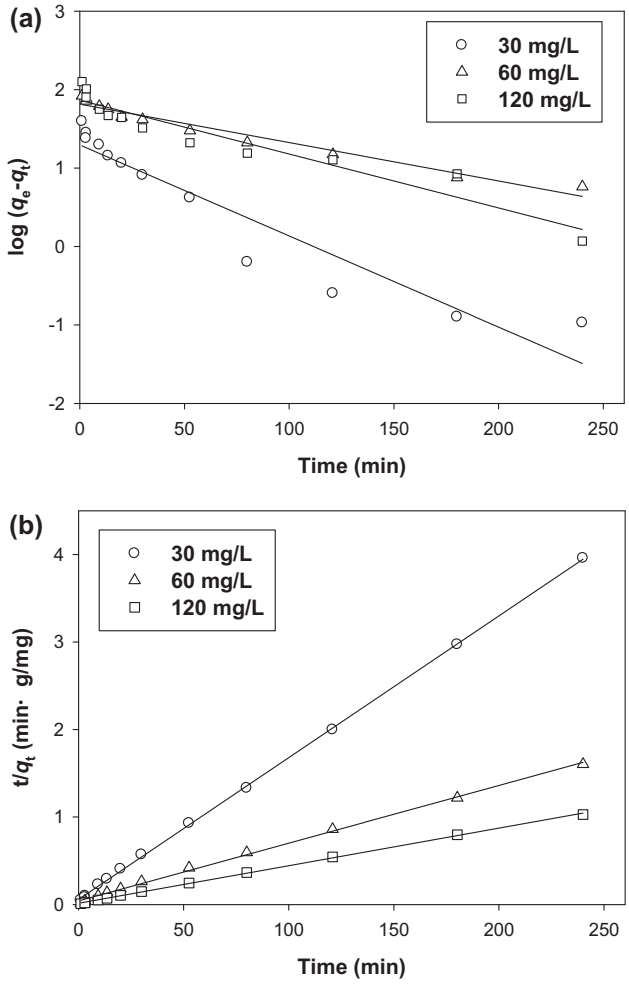

Fig. 11. Simulation of TA adsorption to SBA-15-NH_2 using (a) pseudo-first-order kinetics and (b) pseudo-second-order kinetics.

3.4. Effect of pH and ionic strength on TA adsorption

The influence of solution pH on TA adsorption to SBA-15-NH_2 is presented in Fig. 12. Clearly, TA adsorption to SBA-15-NH_2 observed strongly pH dependent over the examined pH range. The pH-dependency curve was bell-shaped with the peak at pH near 6.0 (nearby the IEP of SBA-15-NH_2 see Fig. 5). The maximum TA adsorption amount was found to be 92.163 mg/g.

TA adsorption to SBA-15-NH_2 was virtually associated with the specific interactions between TA and surface aminopropyl group. At the lower pH range (3–4.5), TA exists in neutral species [1,38]. The hydrogen bonding interaction between the neutral TA species and aminopropyl group accounted for the effective adsorption of TA. At pH 4.5–5.8, TA is dominated by the anionic form and the aminopropyl groups are positively charged by protonation at pH below 9.8 [32]. Electrostatic attraction between dissociated TA molecules and protonated amino groups led to the augmented adsorption. At pH above 5.8, increasing solution pH decreased the protonation of aminopropyl group and reduced the hydrogen bonding interaction between aminopropyl group and

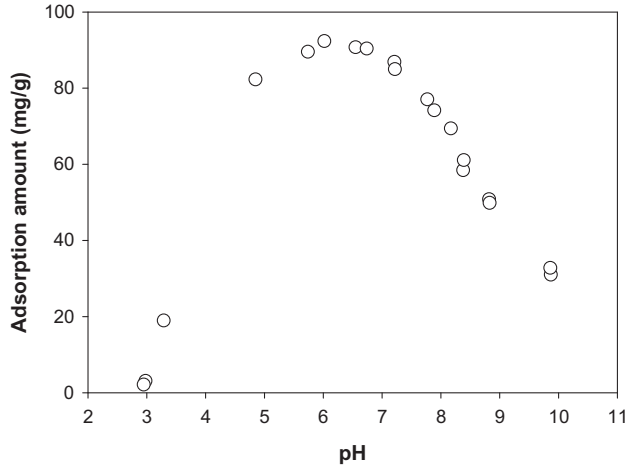

Fig. 12. Effect of solution pH for TA adsorption on SBA-15-NH_2.

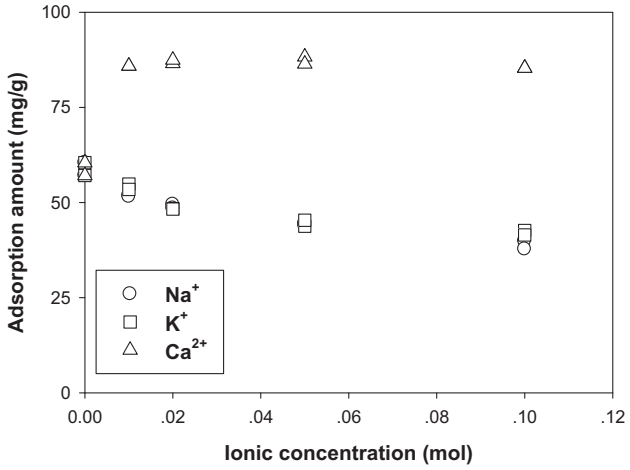

Fig. 13. Effect of ionic strength for TA adsorption to SBA-15-NH_2.

dissociated TA. In addition, SBA-15-NH_2 gradually have negative charge (see IEP in Fig. 5), which decreased electrostatic interaction between adsorbent and dissociated TA resulting in the suppressed TA adsorption.

The effect of ionic strength on TA adsorption is shown in Fig. 13. Clearly, the TA adsorption on SBA-15-NH_2 showed strong dependence of ionic strength. As presented in Fig. 13, changing the ionic strength from 0.01 to 0.1 M with NaCl or KCl, the adsorption of TA on SBA-15-NH_2 was suppressed. However, the added $CaCl_2$ solution enhanced the adsorption and no obvious augment was observed at ionic concentration above 0.02 M (see Fig. 13). It can be rationalized by the fact that increasing ionic strength could reduce the adsorption sites by making the adsorbent shrinkage and decreasing the porosity of the adsorbent [39,40]. Nevertheless, Na^+, K^+, and Ca^{2+} ions could directly interact with TA to form complex compounds, which could enhanced the adsorption of TA to SBA-15-NH_2. The opposite trends of ionic strength effects observed between Na^+, K^+, and Ca^{2+} ions in this study were likely caused by their different abilities in hydrating, ion pairing, and complexing with counterions.

4. Conclusions

In this study, aminopropyl functionalized SBA-15 samples were prepared by the post-grafting method, and the adsorption of TA over the adsorbents was investigated. Characterization results showed that aminopropyl groups were successfully grafted on SBA-15, and both of SBA-15 and SBA-15-NH_2 samples have ordered mesopore structure. In addition, the distribution of aminopropyl groups in the SBA-15 was heterogeneous. SBA-15-NH_2 enhanced TA adsorption dramatically compared with SBA-15 by invoking the hydrogen bonding interaction and electrostatic between surface aminopropyl groups and TA molecules. TA adsorption to the adsorbent followed pseudo-second-order kinetics, and increasing initial concentration results in retarded TA adsorption rate due to prolonged diffusion pathway. In addition, TA adsorption to SBA-15-NH_2 was highly dependent on pH and ionic strength. The findings in this study highlight the potential of aminopropyl functionalized mesoporous materials for adsorptive removal of aqueous TA in drinking water treatment.

Acknowledgements

This work was supported by the Natural Science Foundation of China (Grants 21077050, 21277069 and 51208257), the National High-Tech R&D Program (863 program) of China (Grant 2012AA062607), "Twelfth Five Year Plan" key disciplines of ecology of Jiangsu province.

References

[1] J.H. An, S. Dultz, Adsorption of tannic acid on chitosan-montmorillonite as a function of pH and surface charge properties, Appl. Clay. Sci. 36 (2007) 256–264.
[2] M.Y. Chang, R.S. Juang, Adsorption of tannic acid, humic acid, and dyes from water using the composite of chitosan and activated clay, J. Colloid Interface Sci. 278 (2004) 18–25.
[3] E.De. Nicola, S. Meric, M. Gallo, M. Laccarino, C.D. Rocca, G. Lofrano, T. Russo, G. Pagano, Vegetable and synthetic tannins induce hormesis/toxicity in sea urchin early development and in algal growth, Environ. Pollut. 146 (2007) 46–54.
[4] Y. Tang, S. Liang, S. Yu, N. Gao, J. Zhang, H. Guo, Y. Wang, Enhanced adsorption of humic acid on amine functionalized magnetic mesoporous composite microspheres, Colloid Surf. A 406 (2012) 61–67.
[5] X.G. Zhang, R.A. Minear, Characterization of high molecular weight disinfection byproducts resulting from chlorination of aquatic humic substances, Environ. Sci. Technol. 36 (2002) 4033–4038.
[6] A. Cassano, J. Adzet, R. Molinari, M.G. Buonomenna, J. Roig, E. Drioli, Membrane treatment by nanofiltration of exhausted vegetable tannin liquors from the leather industry, Water. Res. 37 (2003) 2426–2434.
[7] V.P. Vinod, T.S. Anirudhan, Sorption of tannic acid on zirconium pillared clay, J. Chem. Tech. Biotech. 77 (2002) 92–101.
[8] W.W. Li, X.D. Li, K.M. Zeng, Aerobic biodegradation kinetics of tannic acid in activated sludge system, Biochem. Eng. J. 43 (2009) 142–148.
[9] A. Buso, L. Balbo, M. Giomo, G. Farnia, G. Sandonà, Electrochemical removal of tannins from aqueous solutions, Ind. Eng. Chem. Res. 39 (2000) 494–499.

[10] J. Rivera-Utrilla, C. Moreno-Castilla, E. Utrera-Hidalgo, F. Carrasco-Marín, Removal of tannic acid from aqueous solutions by activated carbons, Chem. Eng. J. 52 (1993) 37–39.
[11] T.S. Anirudhan, M. Ramachandran, Adsorptive removal of tannin from aqueous solutions by cationic surfactant-modified bentonite clay, J. Colloid Interface Sci. 299 (2006) 116–124.
[12] J. Wang, A. Li, L. Xu, Y. Zhou, Adsorption of tannic and gallic acids on a new polymeric adsorbent and the effect of Cu(II) on their removal, J. Hazard. Mater. 169 (2009) 794–800.
[13] X.P. Liao, Z.B. Lu, B. Shi, Selective adsorption of vegetable tannins onto collagen fibers, Ind. Eng. Chem. Res. 42 (2003) 3397–3402.
[14] J.S. Beck, J.C. Vartuli, W.J. Roth, M.E. Leonowicz, C.T. Kresge, K.D. Schmitt, C.T.W. Chu, D.H. Olson, E.W. Sheppard, A new family of mesoporous molecular sieves prepared with liquid crystal templates, J. Am. Chem. Soc. 114 (1992) 10834–10843.
[15] C.T. Kresge, M.E. Leonowicz, W.J. Roth, J.C. Vartuli, J.S. Beck, Ordered mesoporous molecular sieves synthesized by a liquid-crystal template mechanism, Nature. 359 (1992) 710–712.
[16] U. Ciesla, F. Schüth, Ordered mesoporous materials, Micropor. Mesopor. Mater. 27 (1999) 131–149.
[17] F. Hoffmann, M. Cornelius, J. Morell, M. Fröba, Silica-based mesoporous organic-inorganic hybrid materials, Angew. Chem. Int. Ed. 45 (2006) 3216–3251.
[18] N.R.E.N. Impens, P. van der Voort, E.F. Vansant, Silylation of micro-, meso- and non-porous oxides: A review, Micropor. Mesopor. Mater. 28 (1999) 217–232.
[19] K. Ariga, A. Vinu, Y. Yamauchi, Q. Ji, J.P. Hill, Nanoarchitectonics for mesoporous materials, Bull. Chem. Soc. Jpn. 85 (2012) 1–32.
[20] D. Tarn, C.E. Ashley, M. Xue, E.C. Carnes, J.I. Zink, C.J. Brinker, Mesoporous silica nanoparticle nanocarriers: Biofunctionality and biocompatibility, Acc. Chem. Res. 46 (2013) 792–801.
[21] D. Gu, F. Schüth, Synthesis of non-siliceous mesoporous oxides, Chem. Soc. Rev. 43 (2013) 313–344.
[22] Q. Tao, Z. Xu, J. Wang, F. Liu, H. Wan, S. Zheng, Adsorption of humic acid to aminopropyl functionalized SBA-15, Micropor. Mesopor. Mater. 131 (2010) 177–185.
[23] K. Ariga, A. Vinu, M. Miyahara, J.P. Hill, T. Mori, One-Pot separation of tea components through selective adsorption on pore-engineered nanocarbon, carbon nanocage, J. Am. Chem. Soc. 129 (2007) 11022–11023.
[24] K. Ariga, A. Vinu, Q. Ji, O. Ohmori, J.P. Hill, S. Acharya, J. Koike, S. Shiratori, A layered mesoporous carbon sensor based on nanopore-filling cooperative adsorption in the liquid phase, Angew. Chem. Int. Ed. 47 (2008) 7254–7257.
[25] J. Wang, S. Zheng, J. Liu, Z. Xu, D. Xu, Tannic acid adsorption on amino-functionalized magnetic mesoporous silica, Chem. Eng. J. 165 (2010) 10–16.
[26] D.Y. Zhao, J.L. Feng, Q.S. Huo, G.D.N. Melosh, G.H. Fredrickson, B.F. Chmelka, G.D. Stucky, Triblock Copolymer Syntheses of Mesoporous Silica with Periodic 50 to 300 Angstrom Pores, Science. 279 (1998) 548–552.
[27] D.Y. Zhao, Q.S. Huo, J.L. Feng, B.F. Chmelka, G.D. Stucky, Nonionic Triblock and Star Diblock Copolymer and Oligomeric Surfactant Syntheses of Highly Ordered, Hydrothermally Stable, Mesoporous Silica Structures, J. Am. Chem. Soc. 120 (1998) 6024–6036.
[28] X.G. Wang, K.S.K. Lin, J.C.C. Chan, S.F. Cheng, Direct synthesis and catalytic applications of ordered large pore aminopropyl-functionalized SBA-15 mesoporous materials, J. Phys. Chem. B. 109 (2005) 1763–1769.
[29] L. Mercier, T.J. Pinnavaia, Direct Synthesis of Hybrid Organic−Inorganic Nanoporous Silica by a Neutral Amine Assembly Route: Structure−Function Control by Stoichiometric Incorporation of Organosiloxane Molecules, Chem. Mater. 12 (2000) 188–196.
[30] J.M. Rosenholm, T. Czuryszkiewicz, F. Kleitz, J.B. Rosenholm, M. Lindén, On the nature of the brønsted acidic groups on native and functionalized mesoporous siliceous SBA-15 as studied by benzylamine adsorption from solution, Langmuir 23 (2007) 4315–4323.
[31] J.M. Rosenholm, M. Lindén, Towards establishing structure-activity relationships for mesoporous silica in drug delivery applications, J. Controlled. Release 128 (2008) 157–164.
[32] J.M. Rosenholm, M. Lindén, Wet-chemical analysis of surface concentration of accessible groups on different amino-functionalized mesoporous SBA-15 silicas, Chem. Mater. 19 (2007) 5023–5034.
[33] J. Magalhes, L. Moreira, U. Rodrigues-Filho, M. Giz, M. Pereira-da-Silva, R. Landers, R. Vinhas, P. Nascente, Surface chemistry of the iron tetraazamacrocycle on the aminopropyl-modified surface of oxidized n-Si(100) by AFM and XPS, Surf. Interface Anal. 33 (2002) 293–298.
[34] S. Deng, R. Bai, Adsorption and desorption of humic acid on aminated polyacrylonitrile fibers, J. Colloid Interf. Sci. 280 (2004) 36–43.
[35] H. Salmio, D. Brühwiler, Distribution of amino groups on a mesoporous silica surface after submonolayer deposition of aminopropylsilanes from an anhydrous liquid phase, J. Phys. Chem. C 111 (2007) 923–929.
[36] H.C. Trivedi, V.M. Patel, R.D. Patel, Adsorption of cellulose triacetate on calcium silicate, Eur. Polym. J. 9 (1973) 525–531.
[37] Y.S. Ho, G. McKay, Pseudo-second order model for sorption processes, Process. Biochem. 34 (1999) 451–465.
[38] J. Wang, C. Zheng, S. Ding, H. Ma, Y. Ji, Behaviors and mechanisms of tannic acid adsorption on an amino-functionalized magnetic nanoadsorbent, Desalination. 273 (2011) 285–291.
[39] D. Xu, X. Zhou, X. Wang, Adsorption and desorption of Ni^{2+} on Na^{+} montmorillonite: Effect of pH, ionic strength, fulvic acid, humic acid and addition sequences, Appl. Clay. Sci. 39 (2008) 133–141.
[40] Q. Lan, A.S. Bassi, J. Zhu, A. Margaritis, A modified Langmuir model for the prediction of the effects of ionic strength on the equilibrium characteristics of protein adsorption onto ion exchange/affinity adsorbents, J. Chem. Eng. 81 (2001) 179–186.